

Levitation force analysis of ring and disk shaped permanent magnet-high temperature superconductor

Sinan Basaran & Selim Sivrioglu*

Department of Mechanical Engineering, Gebze Technical University, Gebze, Turkey

Received 4 February 2016; revised 2 January 2017; accepted 27 February 2017

In superconducting magnetic levitation systems, interaction models between a high temperature superconductor and a permanent magnet are useful to analyze the dynamics of the levitated system. In this study, stiffness equations of a superconducting levitation system using a disk and a ring permanent are obtained using frozen image concept. The variation of the stiffness has been analyzed for vertical movements of the PMs. For engineering applications, accuracy of such models should be tested experimentally. An experimental PM-HTS setup has been built to verify the obtained models for different cooling height conditions. Levitation forces computed using the frozen image approach for the disk and ring PMs are converged to the experimental results when the cooling heights are smaller values.

Keywords: Superconducting magnetic levitation, Frozen image approach, Interaction model

1 Introduction

The technological developments concerning with superconducting magnetic levitation have great advancement especially in energy storage systems and maglev transportation applications¹⁻³. Superconducting magnetic bearing (SMB) has advantages due to passively stable characteristics with considerable stiffness in the radial and axial directions⁴. In bearing applications in mechanical systems, there are two types of bearings configurations considering the loading direction such as radial and axial bearings. If a rotor-PM is located inside a hollow HTS cylinder or a ring HTS, then the resulting levitation structure creates a radial or journal magnetic bearing⁵. The levitation of a permanent magnet over a bulk high temperature superconductor creates an axial type bearing configuration. In most axial type PM-HTS levitation systems, a disk PM is generally used with a rotor element. In some superconducting levitation applications, it is necessary to understand the variation of the levitation forces with different PM shapes.

The interaction models are used to calculate the levitation force and stiffness between PM and HTS. In engineering systems, such models are useful to predict the dynamics of the levitated system. The frozen image approach⁶ was used to calculate the vertical and horizontal levitation forces and

stiffness's. As is well known, the frozen image model does not include hysteresis in the HTS. For small movements of the PM, the frozen image model successfully predicts the force of interaction between the disk PM and the bulk HTS^{7,8}.

The variation of the levitation force for different permanent magnet shapes can be analyzed using current modeling approaches. In this study, a disk PM and a ring PM over a bulk HTS is modeled and stiffness equations are derived for the vertical displacement of PMs. For the proposed disk and ring shaped PM-HTS systems, the stiffness's are computed on the basis of magnetic potentials obtained with the frozen image concept. Some experimental verification are presented and compared with analytical results for decreasing cooling heights of the disk and ring PMs.

2 Interaction Modeling

2.1 Disk PM-HTS levitation system

A disk PM over a bulk HTS is a basic superconducting levitation system as depicted in Fig. 1. Here, Fig. 1(a) shows the PM at cooling position and Fig. 1(b) shows the PM at levitation position. In references^{6,8-10}, the frozen image technique is explained in an ideal situation where the superconductor is a large surface with no dimension and a permanent magnet is levitating above the flat surface. In practice, the HTS has a certain dimension with different shapes. Assuming that the bulk HTS has a large size comparing to the PM, the geometry

*Corresponding author (E-mail: s.selim@gtu.edu.tr)

illustrated in Fig. 1 can be considered within the scope of the frozen image technique. Moreover, a tilt angle θ that occurs in levitation from the vertical due to the inhomogeneities in the magnetism of the PM and the HTS is accepted in the analysis. Note that the tilt angle is considered in cooling phase (Fig. 1(a)) due to the fact that the frozen image is not rotating as well as not moving.

The frozen image approach is applied to the disk PM-HTS levitation system. In this approach, a magnetic dipole is assumed to be located in the geometric center of the PM. A combination of frozen dipole (flux pinning) and mirror dipole (diamagnetic image) appear inside the HTS material. Considering the superconducting levitation system, the total interaction potential U_{tot} of the system is given as:

$$U_{tot} = U_{dia} + U_{fro} \quad \dots (1)$$

where U_{dia} and U_{fro} are the diamagnetic and the frozen image potentials, respectively. Equations of the diamagnetic and frozen image potentials are obtained as:

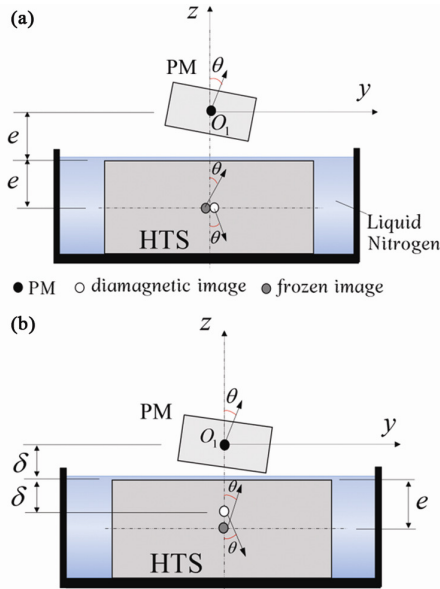


Fig. 1 – Disk PM-HTS levitation system for the frozen image approach (a) cooling phase and (b) levitation phase

$$U_{dia} = \frac{\mu_0 m_{11} m_{12}}{4\pi} \left(\frac{\lambda_1}{(2e-2z)^3} \right) \quad \dots (2)$$

$$U_{fro} = \frac{\mu_0 m_{11} m_{12}}{4\pi} \left[\frac{x^2 \lambda_2 + y^2 \lambda_3 + (2e-z)^2 \lambda_4 - 6\lambda_5 xy - 6\lambda_6 x(2e-z) - 6\lambda_7 y(2e-z)}{(x^2 + y^2 + (2e-z)^2)^{5/2}} \right] \quad \dots (3)$$

Where $\lambda_1, \dots, \lambda_7$ show the trigonometric relations and are derived as $\lambda_1 = 1 + \cos^2 \theta$, $\lambda_2 = 1 - 3\sin^2 \theta \cos^2 \phi$, $\lambda_3 = 1 - 3\sin^2 \theta \sin^2 \phi$, $\lambda_4 = 1 - 3\cos^2 \theta$, $\lambda_5 = \sin^2 \theta \sin \phi \cos \phi$, $\lambda_6 = \sin \theta \cos \theta \cos \phi$ and $\lambda_7 = \sin \theta \cos \theta \sin \phi$, and. Here, θ is the angle between rotational magnetization symmetry axes of the PM with the vertical direction and ϕ is the dipole angle at $x-y$ plane (not seen in Fig. 1). The stiffness in x direction due to vertical displacement of the disk PM is obtained by taking partial derivative of the diamagnetic and the frozen parts and substituting the variables $x = 0$, $y = 0$, $z = \bar{z}$, $\theta = \theta$ and $\phi = \phi$ as follows:

$$k_{xx_disk} = \frac{\partial^2 U_{dia}}{\partial x^2} + \frac{\partial^2 U_{fro}}{\partial x^2} = \frac{\mu_0 m_{11} m_{12}}{4\pi} \left[\frac{2\lambda_2 - 5\lambda_4}{(2e - \bar{z})^5} \right] \quad \dots (4)$$

Also, the stiffness in z direction due to vertical displacement of the disk PM is obtained as:

$$k_{zz_disk} = \frac{\partial^2 U_{dia}}{\partial z^2} + \frac{\partial^2 U_{fro}}{\partial z^2} = \frac{\mu_0 m_{11} m_{12}}{4\pi} \left[\frac{48\lambda_1}{(2e - 2\bar{z})^5} + \frac{12\lambda_4}{(2e - \bar{z})^5} \right] \quad \dots (5)$$

Table 1 shows the magnetic moments and the position vector that used in derivation of the stiffness equations. In Table 1, \vec{m}_{11} is the magnetic moment of the dipole from the disk PM, and \vec{m}_{12} is the magnetic moment of the dipole from the diamagnetic image of

Table 1 – Magnetic moments of the disk PM-HTS system

Images	Magnetic moments	Position vectors
Dipole-diamagnetic	$\vec{m}_{11} = m_{11} (\sin \theta \cos \phi \hat{x} + \sin \theta \sin \phi \hat{y} + \cos \theta \hat{z})$	$\vec{r} = r_x \hat{x} + r_y \hat{y} + r_z \hat{z}$
	$\vec{m}_{12} = m_{12} (\sin \theta \cos \phi \hat{x} + \sin \theta \sin \phi \hat{y} - \cos \theta \hat{z})$	$r_x = 0, r_y = 0, r_z = 2e - 2z$
Dipole-Frozen	$\vec{m}_{11} = m_{11} (\sin \theta \cos \phi \hat{x} + \sin \theta \sin \phi \hat{y} + \cos \theta \hat{z})$	$\vec{r} = r_x \hat{x} + r_y \hat{y} + r_z \hat{z}$
	$\vec{m}_{12} = m_{12} (\sin \theta \cos \phi \hat{x} + \sin \theta \sin \phi \hat{y} + \cos \theta \hat{z})$	$r_x = x, r_y = y, r_z = 2e - z$

\vec{m}_{11} in the HTS. Also, m_{11} and m_{12} are the amplitudes of these vectorial values.

2.2 Ring PM-HTS levitation system

An interaction modeling for a ring shaped PM is not reported in literature. For a disk PM, a magnetic dipole is assumed to be located in the geometric center of the disk PM. Depending on the dipole inside the PM, a combination of frozen and mirror dipole appear inside the HTS material. For a ring shaped PM, if the cross section of the ring is considered, dipoles appear in two sides due to having two geometric centers for the ring HTS. Note that magnetization fields of the ring PM is also two sided in an axisymmetric analysis. Therefore, accepting two dipole moments may be a good approximation in applying frozen image technique to the ring shaped PM.

The ring shaped permanent magnet over a bulk high temperature superconductor at the cooling phase of a superconducting levitation as shown in Fig. 2(a). The ring PM dimension is given by outer diameter, inner diameter and height such as $d_o \times d_i \times h_a$. The coordinate system Oxz is fixed to the PM.

When the bulk HTS is field cooled with the ring PM at a certain cooling height e , two images appear such as the frozen image and the diamagnetic image as shown in Fig. 2(a). The distance of both images from the surface of the HTS is equal to e before levitation is completed. The ring PM loses some

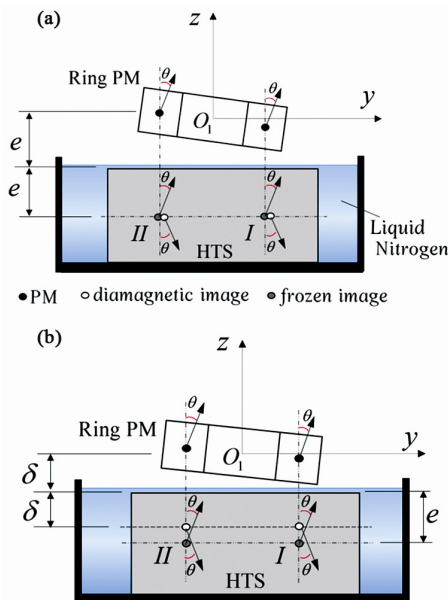


Fig. 2 – Ring PM-HTS levitation system for the frozen image approach (a) cooling phase and (b) levitation phase

height when its supporter is removed after cooling of the HTS is completed. In the levitation phase as shown in Fig. 2(b), while the frozen image is fixed in e , the diamagnetic image moves with the PM and has the levitation height δ from the surface of the ring HTS.

In the ring shaped PM case, PM-HTS interaction is two sided due to hollow shape of the PM. The total magnetic potentials for I and II sides (Fig. 2) are written as¹¹:

$$\begin{aligned} U_{total}^{(I)} &= U_{dia}^{(I)} + U_{fro}^{(I)} \\ U_{total}^{(II)} &= U_{dia}^{(II)} + U_{fro}^{(II)} \end{aligned} \quad \dots (6)$$

where $U_{dia}^{(I)}$ is the dipole and its diamagnetic image potential for I side. Also, $U_{fro}^{(I)}$ is the dipole and its frozen image potential. Equations of each potentials are written as:

$$\begin{aligned} U_{dia}^{(I)} &= \frac{\mu_0 m_{11} m_{12}}{4\pi} \left\{ \frac{\lambda_4}{(2e-2z)^3} \right\} \\ U_{fro}^{(I)} &= \frac{\mu_0 m_{11} m_{12}}{4\pi} \left[\frac{\lambda_2 x^2 + \lambda_3 y^2 + \lambda_4 (2e-z)^2 + 6\lambda_5 xy - 6\lambda_6 x(2e-z) + 6\lambda_7 y(2e-z)}{(x^2 + y^2 + (2e-z)^2)^{3/2}} \right] \\ U_{dia}^{(II)} &= U_{dia}^{(I)} \\ U_{fro}^{(II)} &= \frac{\mu_0 m_{11} m_{12}}{4\pi} \left[\frac{\lambda_2 x^2 + \lambda_3 y^2 + \lambda_4 (2e-z)^2 - 6\lambda_5 xy - 6\lambda_6 x(2e-z) - 6\lambda_7 y(2e-z)}{(x^2 + y^2 + (2e-z)^2)^{3/2}} \right] \end{aligned} \quad \dots (7)$$

The stiffness equations due to the vertical displacement are obtained by taking the partial derivative of the diamagnetic and the frozen parts and substituting the variables $x = 0, y = 0, z = \bar{z}$, $\theta = \theta$ and $\phi = \phi$ respectively. When the ring PM has vertical movement, the stiffness of the ring PM-HTS in x direction is obtained as:

$$\begin{aligned} K_{xx_ring} &= \frac{\partial^2 U_{dia}^{(I)}}{\partial x^2} + \frac{\partial^2 U_{fro}^{(I)}}{\partial x^2} + \frac{\partial^2 U_{dia}^{(II)}}{\partial x^2} + \frac{\partial^2 U_{fro}^{(II)}}{\partial x^2} \\ &= \frac{\mu_0 m_{11} m_{12}}{2\pi} \left[\frac{2\lambda_2 - 5\lambda_4}{(2e-z)^5} \right] \end{aligned} \quad \dots (8)$$

Similarly, the stiffness equation in z direction is derived as

$$\begin{aligned} K_{zz_ring} &= \frac{\partial^2 U_{dia}^{(I)}}{\partial z^2} + \frac{\partial^2 U_{fro}^{(I)}}{\partial z^2} + \frac{\partial^2 U_{dia}^{(II)}}{\partial z^2} + \frac{\partial^2 U_{fro}^{(II)}}{\partial z^2} \\ &= \frac{\mu_0 m_{11} m_{12}}{2\pi} \left[\frac{48\lambda_1}{(2e-2z)^5} + \frac{12\lambda_4}{(2e-z)^5} \right] \end{aligned} \quad \dots (9)$$

Table 2 – Magnetic moments of the ring PM-HTS system		
Images	Part II Magnetic moments	Part I Magnetic moments
Dipole-diamagnetic	$\vec{m}_{11} = m_{11} (\sin \theta \cos \phi \hat{x} + \sin \theta \sin \phi \hat{y} + \cos \theta \hat{z})$	$\vec{m}_{11} = m_{11} (\sin \theta \cos \phi \hat{x} - \sin \theta \sin \phi \hat{y} + \cos \theta \hat{z})$
	$\vec{m}_{12} = m_{12} (\sin \theta \cos \phi \hat{x} + \sin \theta \sin \phi \hat{y} - \cos \theta \hat{z})$	$\vec{m}_{12} = m_{12} (\sin \theta \cos \phi \hat{x} - \sin \theta \sin \phi \hat{y} - \cos \theta \hat{z})$
	Position vectors	Position vectors
	$\vec{r} = r_x \hat{x} + r_y \hat{y} + r_z \hat{z}$ $r_x = 0, r_y = 0, r_z = 2e - 2z$	$\vec{r} = r_x \hat{x} + r_y \hat{y} + r_z \hat{z}$ $r_x = 0, r_y = 0, r_z = 2e - 2z$
Dipole-frozen	Magnetic moments	Magnetic moments
	$\vec{m}_{11} = m_{11} (\sin \theta \cos \phi \hat{x} + \sin \theta \sin \phi \hat{y} + \cos \theta \hat{z})$	$\vec{m}_{11} = m_{11} (\sin \theta \cos \phi \hat{x} - \sin \theta \sin \phi \hat{y} + \cos \theta \hat{z})$
	$\vec{m}_{12} = m_{12} (\sin \theta \cos \phi \hat{x} + \sin \theta \sin \phi \hat{y} + \cos \theta \hat{z})$	$\vec{m}_{12} = m_{12} (\sin \theta \cos \phi \hat{x} - \sin \theta \sin \phi \hat{y} + \cos \theta \hat{z})$
	Position vectors	Position vectors
	$\vec{r} = r_x \hat{x} + r_y \hat{y} + r_z \hat{z}$ $r_x = x, r_y = y, r_z = 2e - z$	$\vec{r} = r_x \hat{x} + r_y \hat{y} + r_z \hat{z}$ $r_x = x, r_y = y, r_z = 2e - z$

Table 2 shows the magnetic moments and the position vector that used in derivation of the Eqs (8) and (9). In Table 2, \vec{m}_{11} is the magnetic moment of the dipole from the ring PM, and \vec{m}_{12} is the magnetic moment of the dipole from the diamagnetic image of \vec{m}_{11} in the HTS. Also, m_{11} and m_{12} are the amplitudes of these vectorial values.

2.3 Levitation forces

In a superconducting levitation system, supporting forces are generated by stiffness effects between superconductor and PM. Levitation forces of the disk PM-HTS and the ring PM-HTS are computed using obtained stiffness equations for different vertical displacements of the PMs. The force equations are defined for the disk and ring PM as follows:

$$\begin{aligned}
 F_{zz_disk} &= (k_{zz_disk})z \\
 F_{zz_ring} &= (K_{zz_ring})z \quad \dots (10) \\
 F_{xx_disk} &= (k_{xx_disk})z \\
 F_{xx_ring} &= (K_{xx_ring})z
 \end{aligned}$$

where z is the vertical displacement. The parameter values of the disk and ring PMs used in levitation force computations are given in Section 3.

Figure 3 shows variation of the levitation forces F_{zz_disk} and F_{zz_ring} when the PMs move from 5 mm to 1 mm in the vertical direction. As seen in this figure, behavior of the vertical levitation forces is nonlinear.

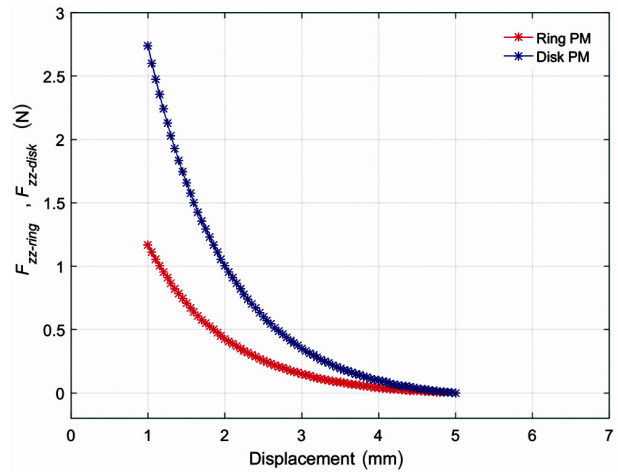


Fig. 3 – Variation of the levitation forces F_{xx_disk} , F_{xx_ring} with the vertical displacement Z

The disk PM produces larger levitation forces than the ring PM due to having higher magnetization value while the surface area of both PMs is almost equal. Variations of the lateral forces F_{xx_disk} , F_{xx_ring} with vertical displacements are shown in Fig. 4. Small increases are observed in the lateral forces with the vertical displacements.

3 Experimental Setup

The structure of the experimental levitation system is schematically depicted in Fig. 5. The levitation system is basically consisted of a bulk HTS, a rotor with attached PM and a non-contact measurement sensor fixed to a support.

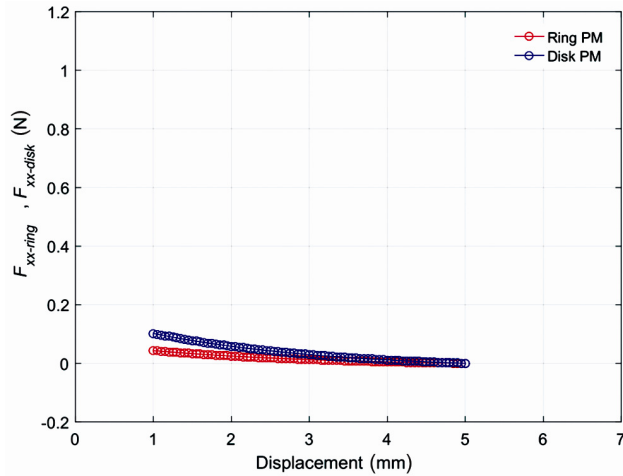


Fig. 4 – Variation of the lateral forces F_{xx_disk} , F_{xx_ring} with the vertical displacement Z

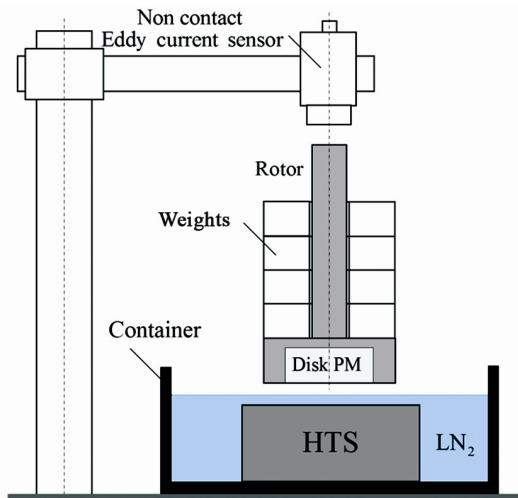


Fig. 5 – Schematic view of the experimental system

The experimental setup is shown in Fig. 6(a,b). The rotor is made from aluminum and its weight 10 g for the ring magnet rotor and 11 g for the disk magnet rotor. The ring masses are made from stainless steel and their weights 12, 2 g for each. To decide the vertical levitation force experimentally, the external ring masses added to the rotor, respectively. The non-contact eddy current type displacement sensor is fixed the top of the rotor for the measurements of the displacements.

The single domain bulk HTS which is 34 mm diameter and 15 mm height is used in experiments. The HTS is fixed to the inside to the Styrofoam insulated container and cooled by the liquid nitrogen. The experiment was carried out by first placing the rotor-PM over the HTS at constant cooling height (CH) which can be adjusted by five different

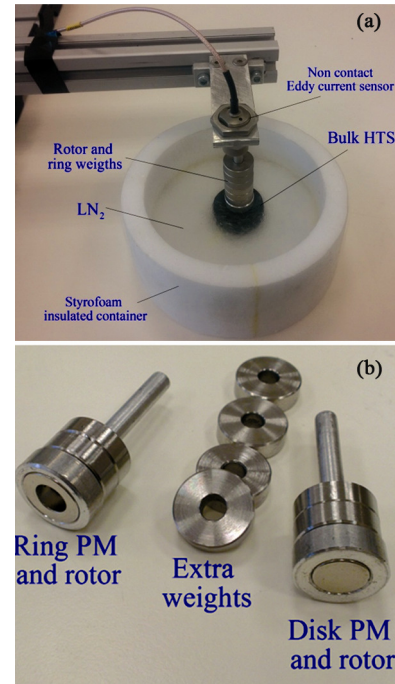


Fig. 6 – Experimental setup (a) complete levitation system and (b) rotors and PMs

supporters. The supporter parts are 15 mm, 10 mm, 5 mm, 3 mm and 2 mm height. After the cooling process by submerged the HTS into liquid nitrogen the supporter parts are separated between PM and HTS.

Permanent magnets have the surface areas of $A_{disk}=0.0113 \text{ m}^2$ and $A_{ring}=0.01264 \text{ m}^2$, respectively. Surface areas of the ring and disk permanent magnets are selected approximately equal to see the effect of the magnet shapes. The ring and the disk PMs are 5 mm thickness both. Magnetization fields of the permanent magnets are computed with axisymmetric analysis using FEMM 4.2 software¹². The ring PM is polarized axially with a magnetization of 0.1369 T and the disk PM is polarized axially with a magnetization of 0.3745 T. The computed magnetization field values are checked with measured values obtained by the gauss meter probe.

4 Results and Discussion

The experimental results are obtained for five different cooling height (CH) condition to understand the dependency of the frozen image based interaction model to the initial cooling gap. The experimental force values are obtained by using the weights and the measured vertical displacements. In all levitation experiments, field cooling (FC) of the HTS is realized. The experimental and analytical

model results are compared for every cooling height condition in figures. The PM-HTS levitation forces are evaluated in terms of experimental and computed results.

The experimental results are given in order of cooling distance from larger to smaller values. Figure 7 illustrates the variation of the vertical force with the displacement using the disk PM in the superconducting levitation experiment established with a starting cooling height of 15 mm. Similarly, the ring PM result is given in Fig. 8 for the same starting cooling height. For the next cooling distance of 10 mm, the results are given for the disk PM and ring PM in Figs 9 and 10, respectively. Either in 15 mm or 10 mm cooling heights, the experimental results partially match with the computed values.

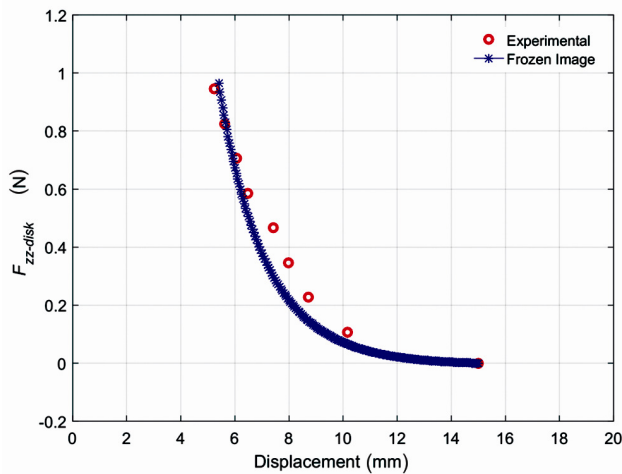


Fig. 7 – Variation of the levitation force with displacement of the disk PM (CH: 15 mm)

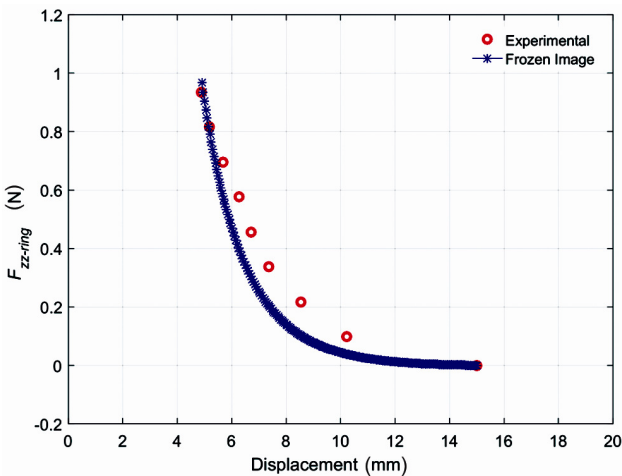


Fig. 8 – Variation of the levitation force with displacement of the ring PM (CH: 15 mm)

Figure 11 shows the variation of the vertical force for the disk PM case from a starting cooling height of 5 mm. Similarly, the ring PM result is given in Fig. 12 for the same starting cooling height. The experimental force results differ from the computed results in both figures but the tendency of experimental results given in Fig. 11 matches with the computed results. The experimental results for the ring PM shown in Fig. 12 does not even show any tendency with the frozen image results like disk PM configuration. This situation is related to the different magnetic field characteristics of the disk PM and ring PM.

For the cooling height of 3 mm, the levitation experiments are repeated for the disk PM and the ring PM. Using the experimental and computed results, Figs 13 and 14 show the variation of vertical forces

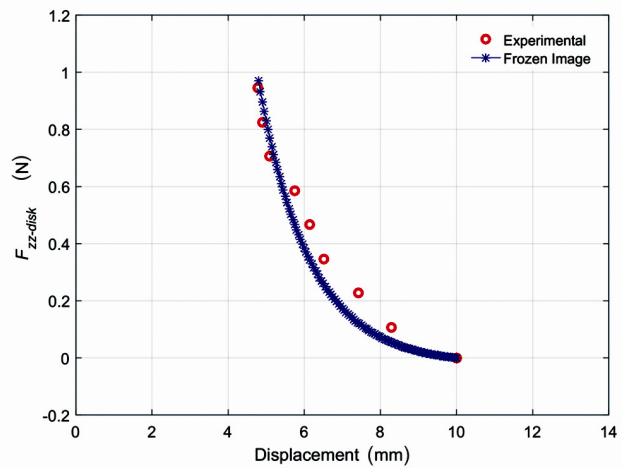


Fig. 9 – Variation of the levitation force with displacement of the disk PM (CH: 10 mm)

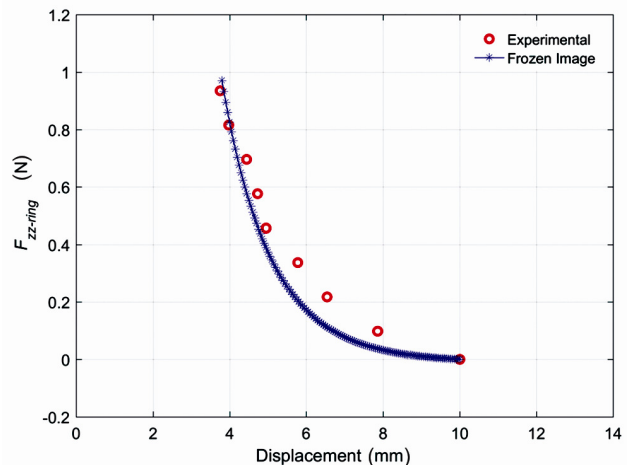


Fig. 10 – Variation of the levitation force with displacement of the ring PM (CH: 10 mm)

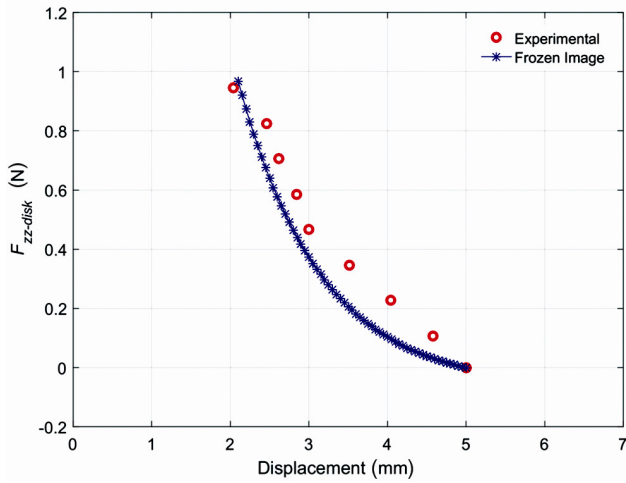


Fig. 11 – Variation of the levitation force with displacement of the disk PM (CH: 5 mm)

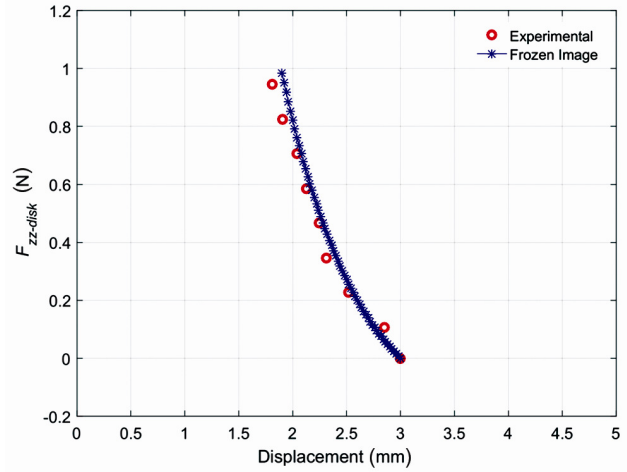


Fig. 13 – Variation of the levitation force with displacement of the disk PM (CH: 3 mm)

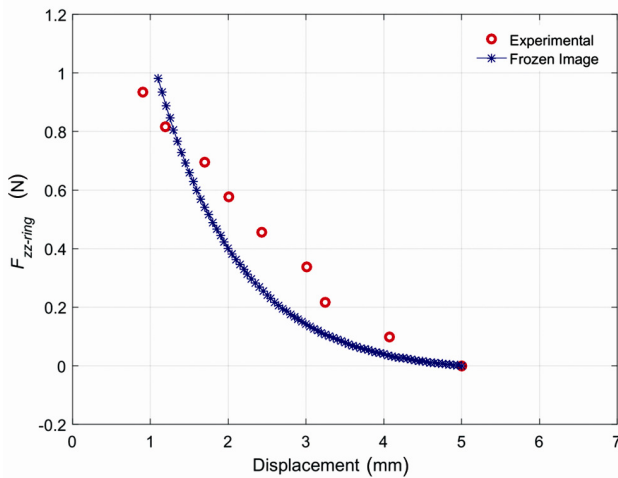


Fig. 12 – Variation of the levitation force with displacement of the ring PM (CH: 5 mm)

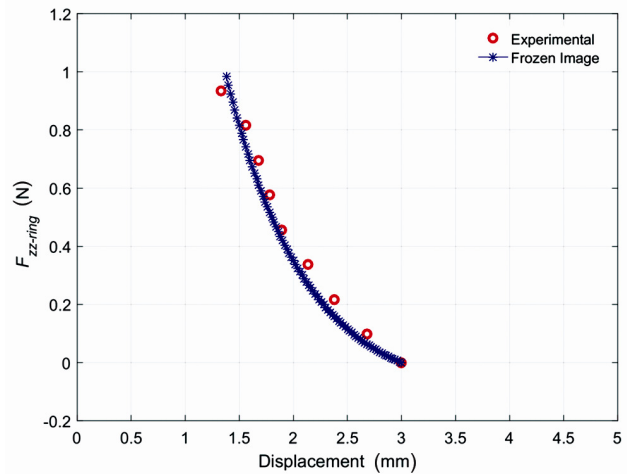


Fig. 14 – Variation of the levitation force with displacement of the ring PM (CH: 3 mm)

for both PMs, respectively. In these results, experimental results match quite closely with the computed values. Figures 15 and 16 are obtained for the cooling height of 2 mm. As seen in these figures, the experimental results perfectly matched with the computed results obtained using frozen image approach.

In most engineering application, the levitation stiffness is considered as a parameter rather than the levitation force. It is possible to have the levitation stiffness for the disk and ring PMs using the same experimental data and computed values for each cooling heights. Although the frozen image model does not include hysteresis, the computed levitation force and stiffness values are very close to measured experimental data at the smaller cooling heights. Also

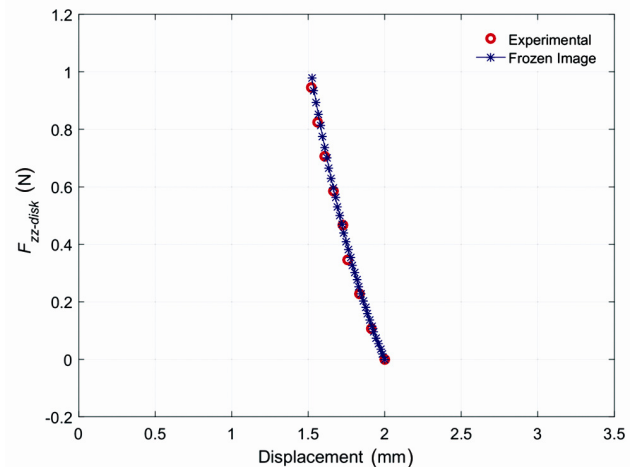


Fig. 15 – Variation of the levitation force with displacement of the disk PM (CH: 2 mm)

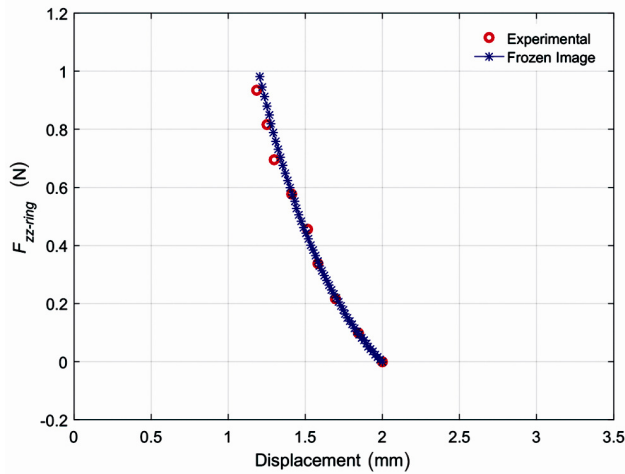


Fig. 16 – Variation of the levitation force with displacement of the ring PM (CH: 2 mm)

it is true that smaller the cooling height larger the levitation stiffness and force.

5 Conclusions

In this research work, the stiffness variation of the disk and ring shaped PM-HTS configurations are presented on the basis of magnetic potential equations obtain for each direction. Evaluation of the frozen image approach is studied using a disk and ring permanent magnet (PM) over a bulk high temperature superconductor (HTS) levitation system for the different cooling height (CH) distances. For smaller cooling heights values, levitation forces computed using the frozen image approach for the disk and ring

PMs are converged to the experimental results. The frozen image model successfully predicts the force of interaction between the PM-HTS.

Acknowledgment

This research study is supported by The Scientific and Technological Research Council of Turkey under the support program of 1001 with the project number 213M581.

References

- 1 Werfel F, Floegel-Delor U, Rothfeld F, Riedel T, Wippich D, Schirrmeister P & Koenig R, *HTS Bulk magnetic application in flywheel energy storage systems FESS and MAGLEV transportation*, Proc Int Conf on MAGLEV, (2014).
- 2 Werfel F, Floegel-Delor U, Rothfeld F, Riedel T, Goebel B, Wippich D & Schirrmeister P, *Supercond Sci Technol*, 25 (2012) 014007.
- 3 Sotelo G G, Dias D H N, Andrade R, Stephan R M, Del-Valle N, Sanchez A, Navau C & Chen D, *IEEE Trans Appl Supercond*, 21(5) (2011) 3532.
- 4 Tang J, Fang J & Tong W, *IEEE Trans Appl Supercond*, 22(6) (2012) 5702109.
- 5 Sivrioglu S & Basaran S, *IEEE Trans Appl Supercond*, 25(4) (2015) 3601507.
- 6 Hull J R & Cansiz A, *J Appl Phys*, 86 (1999) 68.
- 7 Cansiz A, Hull J R & Gundogdu O G, *Supercond Sci Technol*, 18 (2005) 990.
- 8 Cansiz A, *Physica C*, 390 (2003) 356.
- 9 Kordyuk A A, *J Appl Phys*, 83 (1998) 610.
- 10 Hull J R, *Supercond Sci Technol*, 13 (2000) 854.
- 11 Sivrioglu S & Cinar Y, *Supercond Sci Technol*, 20 (2007) 559.
- 12 Meeker D, *Finite Element Method Magnetic*, <http://www.femm.info/wiki/HomePage>.